RSC Advances

ROYAL SOCIETY OF CHEMISTRY

www.rsc.org/advances

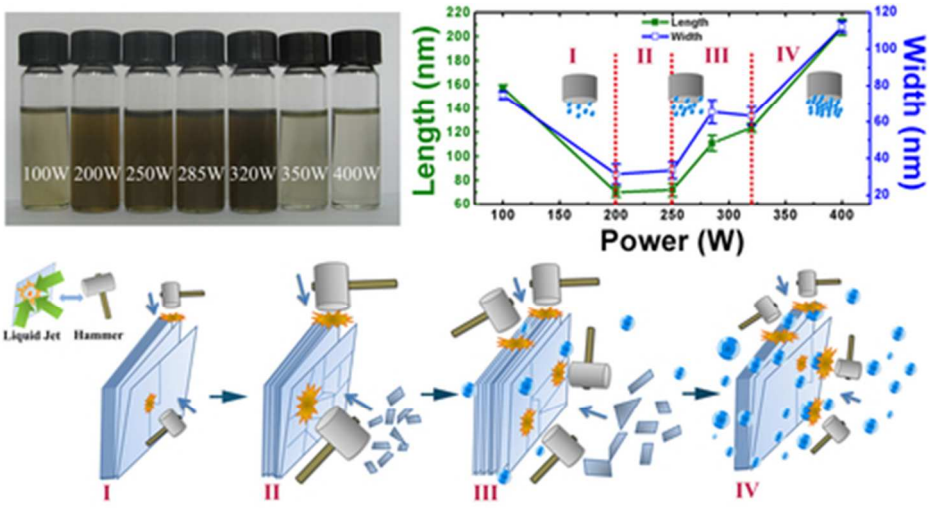

An optimal power to exfoliate MoS2 nanoflakes for high yield and small lateral size with narrow size distribution was obtained.
39x21mm (300 x 300 DPI)

Effects of ultrasonic cavitation intensity on efficient liquid-exfoliation of MoS_2 nanosheets

Wen Qiao[1], Shiming Yan[1, 2], Xuemin He[1], Xueyin Song[1], Zhiwen Li[1], Xing Zhang[1], Wei Zhong[1], and Youwei Du[1]*

[1] National Laboratory of Solid State Microstructures, Department of Physics, Nanjing University, Nanjing 210093, People's Republic of China

[2]College of Science, Henan University of Technology, Zhengzhou 450001, People's Republic of China

Abstract

Liquid exfoliation has been widely used to yield two dimensional layered materials in laboratory because of its simplicity and easy to mass production features. In this study, the dispersions and morphology of exfoliated MoS_2 in N-methyl-2-pyrrolidone (NMP) solvent at different ultrasonic powers are investigated. An optimal power to exfoliate MoS_2 nanoflakes in NMP for high yield and small lateral size with narrow size distribution is obtained. Our results showed that the concentration of dispersions did not increase monotonously with growing ultrasonic power, but rather initially increased with input power, and then decreased after 320 W due to the cavitation shielding effect. The flake size decreased with ultrasonic power from 100 W to 250 W and then increased slightly; after 320 W, the average lateral size of flakes increased dramatically and a wide size distribution with relatively large scale nano-flakes was detected. The mechanism of ultrasonic cavitation effect on the concentration and morphology has been analyzed.

* Corresponding author: wzhong@nju.edu.cn

Introduction

Graphene has shown many fascinating properties as a supplement to silicon-based semiconductor technologies.[1, 2] However, its zero bandgap energy is not suitable for many applications in electronics and optics.[3, 4] Recent developments in transition metal dichalcogenides have shown great promise in filling up the existing gaps.[5, 6] MoS_2 is the most important graphene analogue that has been widely studied. MoS_2 is a quasi-two-dimensional compound, with covalently bonded S-Mo-S single-layers that interact by van der Waals forces.[7, 8] The transition from an indirect bandgap (1.2 eV) in the bulk to a direct bandgap (1.8 eV) in the single-layer leads a dramatic change of properties due to the interlayer interaction.[9] This has attracted interest in a variety of fields, including electronic devices,[5, 10] sensing,[11] luminescence,[12, 13, 14] and catalysis.[15]

Some approaches to obtain few-layered or monolayered MoS_2 have been reported. Original methods utilized to produce MoS_2 nanosheets involve micromechanical exfoliation[13, 16] and lithium intercalation exfoliation.[8, 14, 17] Mechanical cleavage can obtain isolated individual crystal planes (monolayers) with high crystal quality and macroscopic continuity. However, this method can only achieve exfoliation on a small scale. In comparison, lithium intercalation method tends to give sizable quantities of MoS_2 monolayers and its sensitive nature has been overcome by ammonia intercalation reported by Anto Jeffery *et al.* recently,[18] however, it is time-consuming and introduces a phase transformation of MoS_2 from 2H to 1T with Li intercalation.[14, 17] Other approaches that are being explored include chemical vapor deposition (CVD) synthesis[19-21] and liquid exfoliation.[22-25] CVD is a good synthesis method which can give better control over the number of layers and can large-area grow. Nevertheless, it requires high-temperature annealing condition and improved quality of synthesized MoS_2. Liquid exfoliation of layered materials has been found to have great potential for the scalable production of two-dimension (2D) nanosheet-based materials, such as 2D nanosheet suspensions, thin films and 2D

nanosheet-based hybrids and composites.[22-25] Coleman *et al.* have shown that layered materials such as MoS_2, WS_2, and BN can be exfoliated to monolayer and few-layer 2D nanosheets in various organic solvents[22, 25] or aqueous surfactant solutions via sonication.[23]

Liquid exfoliation needs to expose the layered material to ultrasonic waves in a solvent. Such waves generate cavitation bubbles that collapse into high-energy jets, breaking up the layered crystallites and producing exfoliated nanosheets. Ultrasonication has been widely used as a technique for the exfoliation and dispersion nano-materials,[22-27] sonochemical synthesis, ultrasonic cleaning, and lithotripsy.[28-31] Particularly, it has been utilized in the production of two-dimensional materials from bulk layered crystal materials in liquid.[22-27, 32, 33] During the ultrasonic processing, the propagation of high amplitude ultrasonic waves leads to void creation, and the rapid formation of cavities (bubbles). These bubbles grow in the zone of negative pressure of the acoustic field while shrink in the zone of positive pressure. Continued interaction between the bubbles and the acoustic field causes the growth and ultimately violent collapse of the bubbles. The implosion of bubbles can create high-speed jets and intense shock-waves in the surface of bulk materials.[34]

Previous works on liquid exfoliation of layered materials are mainly focused on the effects of solvent selection,[22, 25] sonic time, centrifugal rate, and initial concentration on the exfoliation efficiency,[23, 24] while few researches have been paid on the influences of cavitation intensity induced by ultrasonic on the exfoliation efficiency. [23, 27, 35] Although it is clear that the acoustic cavitation plays a critical role in the exfoliation and dispersion, it is often neglected in previous works. Since the input power of the device is a significant parameter to characterize cavitation, thus in this work, we investigate the influence of different input powers on the dispersion concentration, morphology and photoluminescence (PL) of layered MoS_2.

Experimental Section

Sample preparation

The MoS_2 powder used in these experiments was purchased from Alfa Aesar (CAS 1317-33-5, 41827, 99%). All the experiments were performed by adding 150 mg MoS_2 powder to 20 mL NMP in a 100 mL capacity, flat bottomed beaker. These mixtures were sonicated for 80 min using a 6 mm diameter probe sonic tip (XO-SM50, 900 W, 25 kHz) at 100, 200, 250, 285, 320, 350 and 400 W respectively. The sonic tip was pulsed for 3 s on and 1 s off to avoid damage to the processor and reduce solvent heating and thus degradation. The beaker was connected to a cooling system that allowed for cold water (5℃) to flow around the dispersion during sonication. The dispersions were then centrifuged at 1500 rpm for 45 min. The top 3/4 of the dispersion was collected by pipette for each sample. Then the dispersions were centrifuged at 2000 rpm for 45 min again, at last the top 1/2 of the supernatant containing ultrafine MoS_2 layers was collected.

Characterization methods

The absorbance spectra of the MoS_2 nanoflakes were examined using a spectrophotometric system of Double beam UV visible spectrophotometer (TU-1901). Atomic force microscope (AFM) images were obtained using Scanning Probe Microscopy (Veeco Dimension V, USA). The sample of diluted dispersion was dropped on Si substrate and evaporated at room temperature. The measurements were performed in a tapping mode with standard Si tips (TESP, 270 kHz). The morphology of the samples was examined by transmission electron microscopy (TEM) (Model JEOL-2010, Japan) operated at an accelerating voltage of 120 kV. As a specimen support for TEM investigations, a copper grid covered by a thin transparent carbon film was used. All the samples were diluted range from 3 to 15 times by alcohol and then dropped on copper grids. The crystal structure of 2D nanoflakes was characterized using HRTEM and selected area electron diffraction (SAED). The photoluminescence (PL) spectra were obtained at ambient conditions by a spectrofluorophotometer (Shimadzu RF-5301PC) using Xe lamp as light source at multiple excitation wavelengths of 300, 325, 350, 375, 400, 425, 450, 475 and 500 nm.

Results and Discussion

A probe sonic tip was used to prepare a series of MoS_2 dispersions in N-methyl-2-pyrrolidone (NMP) at different power intensities. The optical properties of the dispersions were studied in detail by measuring their UV-vis absorption spectra. As shown in Figure 1(a), the peaks at 403 nm, 450 nm, 614 nm, and 674 nm are the characteristic absorption bands of exfoliated MoS_2 in solution. The peaks at 674 nm and 614 nm are ascribed to A and B excitonic peaks respectively, arising from the K point of the Brillouin zone in 2D MoS_2.[9] The threshold at~450 nm (C) and ~403 nm (D) could be attributed to the direct transition from the deep valence band to the conduction band.[36, 37] The absorption peaks in the near-UV region (λ < 300 nm) can be explained by the excitonic features of small lateral size of MoS_2 in the sample.[37]

To estimate the concentration, the scattering background is extrapolated from the high-wavelength region (dash line in the inset of Figure 1(a)), and the value of *A/l* solely due to resonant absorption is estimated for each sample (about 674 nm, illustrated by A peaks in Figure 1(a)). In most cases, this allows us to determine the concentration of MoS_2 dispersions regardless of the value of the scattering exponent. The concentration of dispersed material can be semi-quantitatively determined by *A/l* subtracted background, provided the absorption coefficient, α, is known.[24] The *A/l* values subtracted the scattering background as a function of input power are presented in Figure 1(b). It can be seen that the dispersion concentration increases initially with ultrasonic power, and then sharply decreases after 320 W, which completely coincide with the photograph of suspensions of MoS_2 in NMP at various power intensities as shown in Figure 1(d). The color of the final dispersions varies evidently with different powers, indicating that the concentrations of the nanosheets have indeed changed. This difference can be largely attributed to the ultrasonic cavitation effect. For a general liquid, the cavitation intensity increases initially with increasing ultrasonic power, however, it tends to a maximum when the ultrasonic intensity reaches a certain value. The cavitation intensity decreases with further increasing input power. This is because a large number of vain bubbles

generated from the increased ultrasonic power would increase the scattering attenuation and reduce the cavitation intensity.[38] A detailed discussion about the cavitation effects on producing MoS_2 nanoflaks will be presented in Figure 4.

On the other hand, these spectra appear to be superimposed on a power law background in the inset of Figure 1(a). The low-energy non-resonant region appears almost linear hallmarking the light scattering ($\propto \lambda^{-n}$). [22, 24] The scattering exponent, *n*, is estimated from the high wavelength region as plotted in Figure 1(c). It is clear that the scattering exponent, n, is not a constant; but increases from n = 3.5 to n = 3.9 as the ultrasonic power increasing from 100 W to 200 W and then decreases n = 2.7 as the ultrasonic power further increasing to 400 W, suggesting a variation in flake size. The scattering exponent is close to 4.0 from 200 W to 320 W. This might be expected for Rayleigh scattering,[24] which would be consistent with the small lateral size of nanosheets. In addition, the scattering exponent decreases with further increasing power, indicating the increase of flake size. A similar trend is observed at the variation of A excitonic peak position which indicates the change of nanoflakes size, as shown in the inset of Figure 1(c). The blue shift of A peaks shows that the flakes have a relatively smaller dimension.[39]

We performed transmission electron microscopy (TEM) on each sample to determine the quality and dimensions of the flakes. Generally, the flakes appear to be well exfoliated (Figure 2) with some very thin sheets, including monolayers (as shown in the inset of Figure 2(a)). Further examination of the flake quality was performed by selected area electron diffraction (SAED) pattern (Figure 2(b)) and high resolution TEM (HRTEM) images (Figures 2(c) and (d)). Figure 2(b) presents the SAED pattern taken from the MoS_2 flakes selected in Figure 2(a) using a black circle. The SAED pattern indicates the single crystalline nature and an undistorted lattice of the nanoflakes. The high resolution images in Figures 2(c) and (d) show clean, well-defined, hexagonal symmetric structures. The d_{100} is 2.7 Å, and d_{110} is 1.6 Å. These images indicate that high power intensity did not damage or disrupt the hexagonal structure of MoS_2.

Figure 3 displays the TEM micrographs of different samples, suggesting that the MoS_2 is well exfoliated below 320 W. The size of the flakes could be determined readily from large-scale TEM micrographs. As shown in Figure 4(b), the flakes prepared at 100 W have a mean length $\langle L \rangle \approx 157$ nm and width $\langle W \rangle \approx 75$ nm. As the power increased, the flake sizes decrease, reaching $\langle L \rangle \approx 72$ nm and $\langle W \rangle \approx 33$ nm for 250 W sample. However, the flake sizes increase after 250 W, reaching $\langle L \rangle \approx 124$ nm and $\langle W \rangle \approx 63$ nm for 320 W sample and further increasing to $\langle L \rangle \approx 207$ nm and $\langle W \rangle \approx 112$ nm for 400 W sample.

This variation is mainly associated with the ultrasonic cavitation effect. It is generally known that there are two types of acoustic cavitation in liquid as shown in Figure 4(a). Stable cavitation (top in Figure 4(a)) is typically generated at low acoustic fields, whereby bubbles have a long growth cycle and undergo multiple oscillations at the equilibrium position.[40] When the resonance frequency of bubbles corresponds with that of sound wave, the maximum energy coupling of acoustic field and bubbles will be generated, accompanying obvious cavitation effect. In contrast to stable cavitation, inertial cavitation (bottom in Figure 4(a)) will occur when the ultrasonic power future increases, whereby bubbles oscillate and ultimately collapse chaotically within a few sound wave cycles, meanwhile producing extremely high fluid acceleration and broadband noise.[41] Figure 4(c) shows the schematic representation of the exfoliation procedure at different input powers during which the high speed liquid jet is compared to a hammer knocking on the right and profile side of the bulk material. At low input power (Figure 4(c), I), corresponding to the stable cavitation, the knocking on right side has little ability to destroy the covalently bonded S-Mo-S while the knocking profile can easily overcome van der Waals forces holding between sheets. Thus large size of MoS_2 flakes are produced in this region. Decrease in the size of flake with increasing input power is explained by the inertial cavitation, which has the ability to destroy the covalently bonded S-Mo-S and knock the sheets into small flakes along the defects generated by the continuously high intensity knocking on the surface, as shown in (Figure 4(c),

II). The strongest cavitation effect emerges in range from 200 W to 250 W and produces the smallest size nanoflakes with narrow lateral size distribution. This effect is in analogy with the results that the flakes could be cut by the scission of low-energy ball milling and sonication as observed previously for MoS_2 dispersions.[42] It has the same mechanism in the range of 285 W to 320 W. The increase in the number of cavitation bubbles leads to high yield of nanoflakes. But at the same time a small amount of vain bubbles are generated, weakening the knocking intensity and leading to slight increase in size (Figure 4(c), III). For the 400 W sample (Figure 4(c), IV), the flake dimensions reach to a maximum. This is because the ultrasonic cavitation shielding effect, where the increasing population of bubbles beneath the tip hinders the transmission of acoustic waves and the generation of inertial cavitation,[38] resulting in less efficient exfoliation of MoS_2. The photographs of cavitation bubbles in Figure 4(d) are in accordance with the analysis discussed above. An obvious transformation from stable cavitation to inertial cavitation can be observed from the bubbles shown in photographs of 100 W and 200 W. Larger than 285 W, the number of vain bubbles increases with increasing power intensity. Figure 4(e) displays the SEM images of MoS_2 sediments dried at 60 ℃ after the first centrifugation. The size and morphology of these sediments are also largely consistent with our analysis.

Tapping mode atomic force microscopy (AFM) is used for assessing the thicknesses of these 2D MoS_2 layers prepared at different powers. As shown in Figures 5(a), (c) and (e), a clear step of ~3.4, 2.7, 4.4 and 1.4 nm are observed in typical 2D liquid-exfoliated MoS_2 flakes respectively. It is also seen that the 2D nanoflakes display various thickness distributions, but the majority of thickness ranging from 3-7 nm, 1-5 nm and 2-10 nm for 100, 250 and 400 W MoS_2 samples (as shown in Figures 5(b), (d) and (f)), indicating the presence of monolayers in effective exfoliation samples.

As the lateral dimensions of these MoS_2 nanoflakes are mostly smaller than 100 nm, their PL properties are expected to be different from those of samples with relatively larger lateral

dimensions (generally larger than 1 μm). The PL spectra of these nanoflakes were measured using fluorescence spectroscopy at different excitation wavelengths ranging from 325 to 500 nm to provide a comprehensive view of the PL properties of the MoS_2 nanoflakes. Figures 6(a) and (c) show the PL spectra of 2D MoS_2 nanoflakes prepared at 250 W and 400 W respectively. For the excitation wavelength of 375 nm, both samples show a strong luminescence peak centered at ~477 nm and 485 nm respectively. The luminescence becomes less significant at 500 nm excitation wavelengths for both samples. This result is consistent with those of MoS_2 quantum dots and low-dimensional liquid exfoliated MoS_2 flakes.[35, 37, 39, 43, 44]

Less substantial red shift is noticed in the PL spectra of 250 W sample (Figure 6(a)) when the excitation wavelength increases from 325 nm to 500 nm, which may be ascribed to the narrow lateral size distribution. As shown in Figure 6(b), the main lateral dimension ranges from 15 to 35 nm and the full width at half maximum (FWHM) is 34 nm given by Gauss fitting. However, A clear red shift in the PL spectra of 400 W sample (Figure 6(c)) is observed with the increase of the excitation wavelength, which is similar to several recent results.[35, 37, 39, 44] Compared to the 250 W sample, there are a wide lateral size distribution ranged from 20 to 120 nm (FWHM is 88 nm) for the 400 W sample (Figure 6(d)). It is suggested that the excitation dependent PL could be related to the polydispersity of 2D MoS_2 nanoflakes, for which the emission wavelength of the PL is a strong function of the lateral dimension of the quasi-2D nanoflakes due to the quantum size effect.[44]

Conclusions

In conclusion, we have studied the effects of ultrasonic input power on the exfoliate efficiency, morphology and optical property of MoS_2 in solvent NMP based on the cavitation effect. We obtained the high dispersed concentration of the samples produced in the range from 200 W to 320 W, while the smallest later size was mainly less than 60 nm and had a narrow distribution for 250 W sample. An optimal power to exfoliate MoS_2 nanoflakes in NMP for high yield and

small lateral size with narrow size distribution was obtained. Both the narrow and wide size distribution samples were characterized by PL spectroscopy. This work contributes a simple method to the large-scale preparation of small nanoflakes using ultrasonic cavitation effect, which can be possibly extended to other layered materials and be useful for future preparation of MoS_2 quantum dots that utilized in medicine and biology fields given to their low toxicity.

Acknowledgements

This work is financially supported by the National Natural Science Foundation (Grant No. 11174132), the National Key Project for Basic Research (Grant Nos. 2011CB922102 and 2012CB932304). The authors thank Mingjie Li (Department of Chemistry, National University of Singapore) for useful discussion, the assistance of Jinlong Gao, Huimin Li, and Fuchi Liu in conducting the AFM, TEM and PL spectra measurements and the help of Wenbin Xia for photographs.

References

1 K. S. Novoselov, A.K. Geim, S.V. Morozov, D. Jiang, Y. Zhang, S.V. Dubonos, I.V.Grigorieva, A.A. Firsov, *Science*, 2004, 306, 666-669.

2 A. Rycerz, J. Tworzydlo, C. W. J. Beenakker, *Nature Phys.*, 2007, 3, 172-175.

3 T. Palacios, *Nature Nanotech.*, 2011, 6, 464-465.

4 M. Osada, T. Sasaki, *Adv. Mater.*, 2012, 24, 209-209.

5 B. Radisavljevic, A. Radenovic, J. Brivio, V. Giacometti, A. Kis, *Nature Nanotech.*, 2011, 6, 147-150.

6 F. Schwierz, *Nature Nanotech.*, 2011, 6, 135-136.

7 Q. H. Wang, K. Kalantar-zadeh, A. Kis, J. N. Coleman, M. S. Strano, *Nature Nanotechnol.*, 2012, 7, 699–712.

8 H. S. S. Ramakrishna Matte, A. Gomathi, A. K. Manna, D. J. Late, R. Datta, S. K. Pati, C. N. R. Rao, *Angew. Chem., Int. Ed.* 2010, 49, 4059-4062.

9 K. F. Mak, C. Lee, J. Hone, J. Shan, T. F. Heinz, *Phys. Rev. Lett.*, 2010, 105, 136805.

10 O. Lopez-Sanchez, D. Lembke, M. Kayci, A. Radenovic, A. Kis, *Nature Nanotech.* 2011, 8, 497-501.

11 F. K. Perkins, A. L. Friedman, E. Cobas, P. M. Campbell, G. G. Jernigan, and B. T. Jonker, *Nano Lett.*, 2013, 13, 668-673.

12 R. S. Sundaram, M. Engel, A. Lombardo, R. Krupke, A. C. Ferrari, Ph. Avouris, and M. Steiner, *Nano Lett.*, 2013, 13, 1416-1421.

13 A. Splendiani, L. Sun, Y. Zhang, T. Li, J. Kim, C. Chim, G. Galli, F. Wang, *Nano Lett.*, 2010, 10, 1271-1275.

14 G. Eda, H. Yamaguchi, D. Voiry, T. Fujita, M. Chen, M. Chhowalla, *Nano Lett.*, 2011, 11, 5111-5116.

15 D. Voiry, M. Salehi, R. Silva, T. Fujita, M. Chen, T. Asefa, V. B. Shenoy, G. Eda, M. Chhowalla, *Nano Lett.*, 2013, 13, 6222-6227.

16 K. S. Novoselov, D. Jiang, F. Schedin, T. J. Booth, V. V. Khotkevich, S. V. Morozov, and A. K. Geim, *Proc. Natl. Acad. Sci.*, 2005, 102, 10451-10453.

17 P. Joensen, R. F. Frindt, S. R. Morrison, *Mat. Res. Bull.*, 1986, 21, 457-461.

18 A. A. Jeffery, C. Nethravathi, and M. Rajamathi, *J. Phys. Chem. C*, 2014, 118, 1386−1396.

19 K. Liu, W. Zhang, Y. Lee, Y. Lin, M. Chang, Ch.uan Su, Ch. Chang, H. Li, Y. Shi, H. Zhang, Ch. Lai, L. Li, *Nano Lett.*, 2012, 12, 1538-1544.

20 S. Najmaei, Zh. Liu, W. Zhou, X. Zou, G. Shi, S. Lei, B. I. Yakobson, J. Idrobo, P. M. Ajayan1, J. Lou, *Nature Mater.*, 2013, 12, 754-759.

21 Y. Shi, W. Zhou, A. Lu, W. Fang, Y. Lee, A. L. Hsu, S. M. Kim, K. K. Kim, H. Y. Yang, L. Li, J. Idrobo, J. Kong, *Nano Lett.*, 2012, 12, 2784-2791.

22 J. N. Coleman, M. Lotya, A. O'Neill, S. D. Bergin, P. J. King, U. Khan, K. Young, A. Gaucher, S. De, R. J. Smith, I. V. Shvets, S. K. Arora, G. Stanton, H. Y. Kim, K. Lee, G. T. Kim, G. S. Duesberg, T. Hallam, J. J. Boland, J. J. Wang, J. F. Donegan, J. C. Grunlan, G. Moriarty, A. Shmeliov, R. J. Nicholls, J. M. Perkins, E. M. Grieveson, K. Theuwissen, D. W. McComb, P. D. Nellist, V. Nicolosi, *Science*, 2011, 331, 568– 571.

23 R. J. Smith , P. J. King , M. Lotya , C. Wirtz , U. Khan , S. De , A. O'Neill , G. S. Duesberg , J. C. Grunlan , G. Moriarty , J. Chen , J. Wang , A. I. Minett , V. Nicolosi , J. N. Coleman, *Adv. Mater.*, 2011, 23, 3944-3948.

24 A. O'Neill, U. Khan, J. N. Coleman, *Chem. Mater.*, 2012, 24, 2414-2421.

25 G. Cunningham, M. Lotya, C. S. Cucinotta, S. Sanvito, S. D. Bergin, R. Menzel, M. S. P. Shaffer, J. N. Coleman, *ACS Nano*, 2012, 6, 3468-3480.

26 A. Sesis, M. Hodnett, G. Memoli, A. J. Wain, I. Jurewicz, A. B. Dalton, J. D. Carey, G. Hinds, *J. Phys. Chem. B*, 2013, 117, 15141-15150.

27 J. T. Han, J. I. Jang, H. Kim, J. Y. Hwang, H. K. Yoo, J. S. Woo, S. Choi, H. Y. Kim, H. J. Jeong, S. Y. Jeong, K. Baeg, K. Cho, G. Lee, *Scientific Reports*, 2014, 4, 5133:1-7.

28 D. G. Shchukin, E. Skorb, V. Belova, H. Mo ̈hwald, *Adv. Mater.*, 2011, 23, 1922–1934.

29 H. Xu, B. W. Zeiger, K. S. Suslick, *Chem. Soc. Rev.*, 2013, 42, 2555-2567.

30 W. D. O'Brien Jr., *Prog. Biophys. Mol. Biol.*, 2007, 93, 212-255.

31 D. Chen, S. K. Sharma, A. Mudhoo, Handbook on applications of ultrasound: sonochemistry for sustainability (CRC Press, 2011).

32 Y. Hernandez, V. Nicolosi, M. Lotya, F. M. Blighe, Z. Sun, S. De, I. T. Mcgovern, B. Holland, M. Byrne, Y. K. Gunko, J. J. Boland, P. Niraj, G. Duesberg, S. Krishnamurthy, R. Goodhue, J. Hutchison, V. Scardaci, A. C. Ferrari, J. N. Coleman, *Nature*

Nanotech., 2008, 3, 563-568.

33 V. Nicolosi, M. Chhowalla, M. G. Kanatzidis, M. S. Strano, J. N. Coleman, *Science*, 2013, 340, 1226419:1-18.

34 K. S. Suslick, Sonochemistry. *Science*, 1990, 23, 1439-1445.

35 V. Stengl, J. Henych, *Nanoscale*, 2013, 5, 3387–3394.

36 J. P. Wilcoxon, G. A. Samara, *Phys. Rev. B*, 1995, 51, 7299-7302.

37 D. Gopalakrishnan, D. Damien, M. M. Shaijumon, *ACS Nano*, 2014, *8*, 5297-5303.

38 V. S. Sutkar, P. R. Gogate, *Chem. Eng.*, 2009, 155, 26-36.

39 Y. Wang, J. Z. Ou, S. Balendhran, A. F. Chrimes, M. Mortazavi, D. D. Yao, M. R. Field, K. Latham, V. Bansal, J. R. Friend, S. Zhuiykov, N. V. Medhekar, M. S. Strano, K. Kalantar-zadeh, *ACS Nano*, 2013, 7, 10083-10093.

40 M. Ashokkumar, J. Lee, S. Kentish, F. Grieser, *Ultrason. Sonochem.*, 2007, 14, 470-475.

41 W. Lauterborn, T. Kurz, *Rep. Prog. Phys.*, 2010, 73, 106501-106589.

42 Y. Yao, Z. Lin, Z. Li, X. Song, K. Moon, C. Wong, *J. Mater. Chem.*, 2012, 22, 13494-13499.

43 K. Zhou, Y. Zhu, X. Yang, J. Zhou, C. Li, *ChemPhysChem*, 2012, 13, 699–702.

44 J. Z. Ou, A. F. Chrimes, Y. Wang, S. Tang, M. S. Strano, K. Kalantar-zadeh, *Nano Lett.*, 2014, 14, 857−863.

Figures

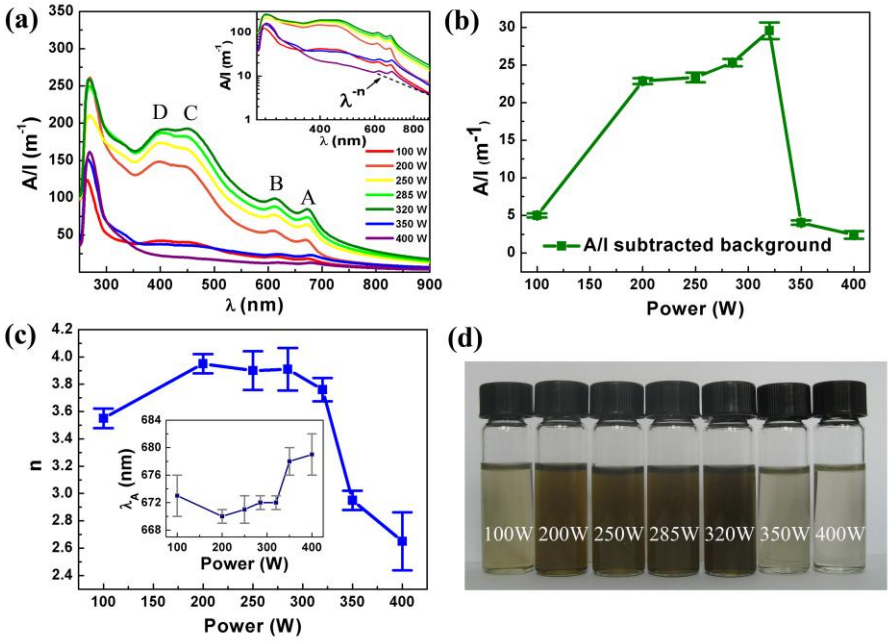

Figure 1. Dispersions of MoS_2 prepared per different ultrasonic power intensities. (a) UV-vis absorption spectra of MoS_2 dispersions in NMP prepared with 100, 200, 250, 285, 320, 350 and 400 W respectively. In all cases the spectra are shown as measured absorbance, *A*, divided by cell length, *l*. Inset in (a) shows the same spectra on a log-log scale. A straight dash line in the high wavelength region of this plot is indicative of a scattering background ($\propto \lambda^{-n}$). (b) *A/l* subtracted background for each sample of A excitonic peak is plotted as a function of ultrasonic power. (c) Scattering exponent, *n*, as a function of ultrasonic power. Inset in (c) shows the variation of the position of A excitonic peaks (λ_A). (d) Photograph of the final dispersions after standing several weeks.

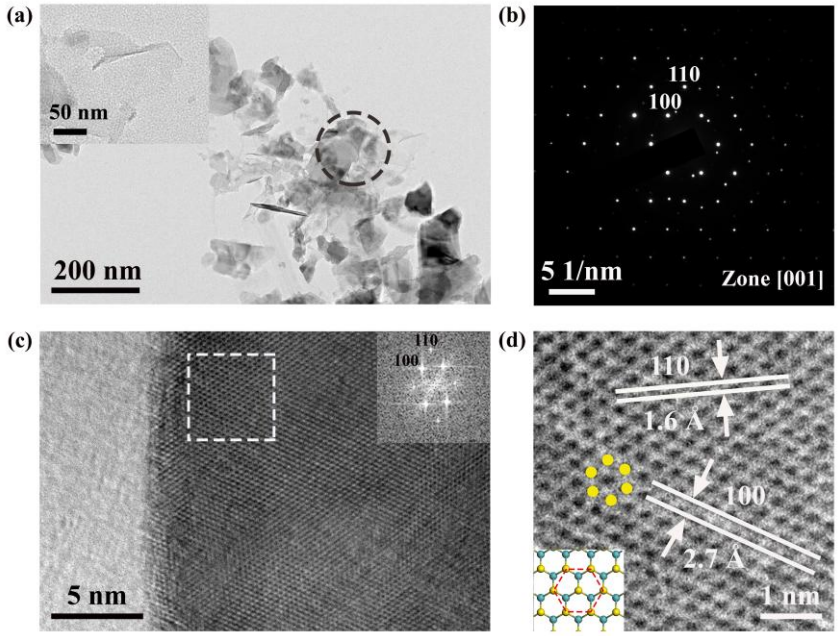

Figure 2. TEM micrographs of dispersion produced at 320 W. (a) A typical bright field TEM image of MoS_2 nanoflakes. Inset: monolayer nanoflake of MoS_2. (b) SAED pattern from the area indicated by the black circle in (a). (c) Phase contrast HRTEM image of a MoS_2 flake. Inset is the Fast Fourier Transform (FFT) pattern of the marked area. (d) A zoomed image of the region in (c) indicated by the white square showing the MoS_2 atomic structure.

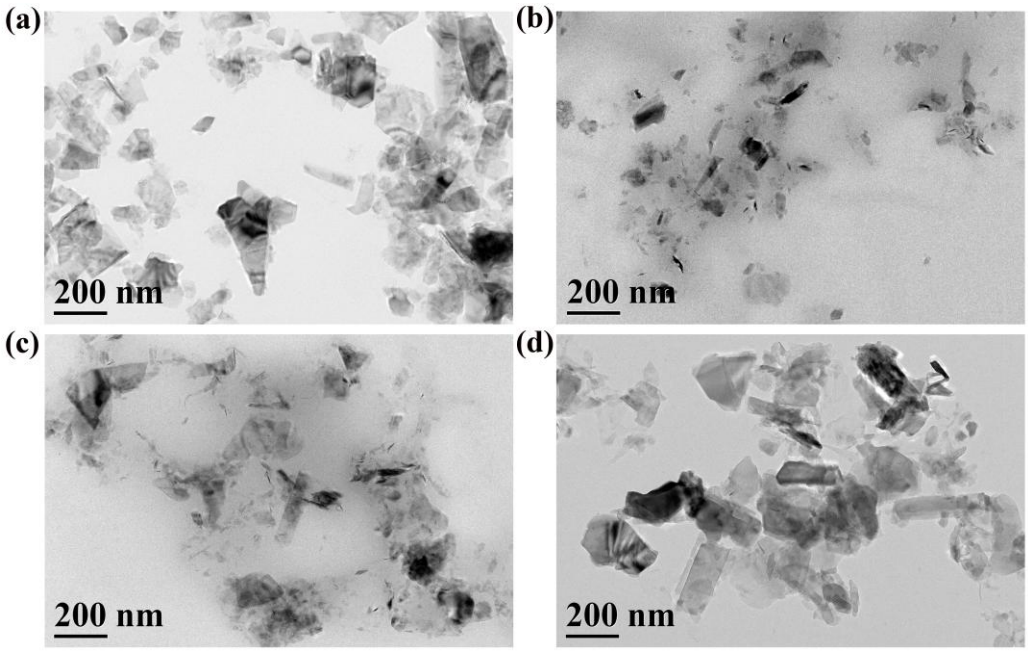

Figure 3. (a) to (d) Typical bright field TEM images of MoS_2 nanoflakes prepared with 100, 250, 320 and 400 W respectively.

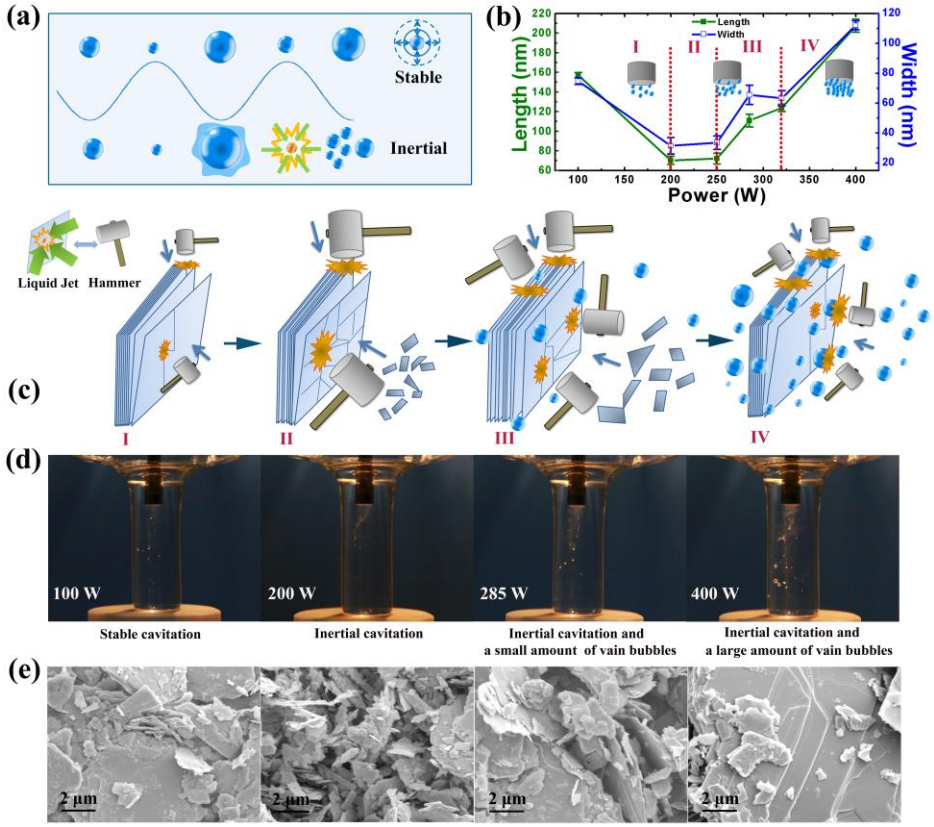

Figure 4. (a) Illustration of the two types of cavitation mechanism. (b) Mean flake length and width (based on more than 300 randomly selected nanoflakes for each sample) per different ultrasonic power intensities. (c) Schematic representation of the exfoliation procedure to obtain MoS_2 nanoflakes in four distinct regions (I to IV). (d) Photographs of the acoustic cavitation bubbles in NMP solvent at different input powers. (e) SEM images of the sediment after centrifugation of 100, 200, 285, 400 W samples.

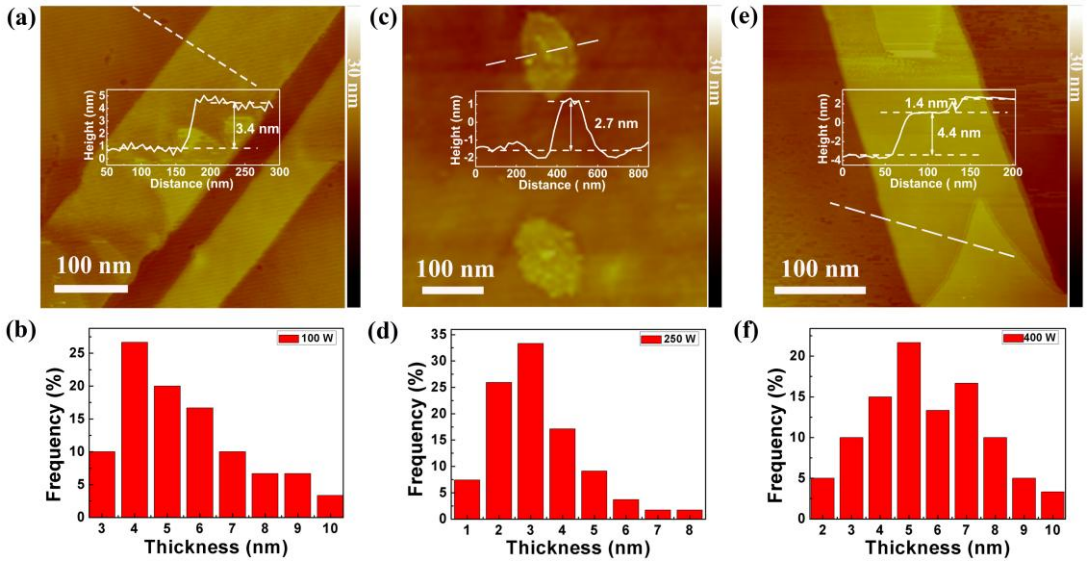

Figure 5. (a), (c) and (e) AFM images and section height profiles of MoS_2 nanoflakes prepared with 100, 250 and 400W. (b), (d) and (f) Thickness distributions based on 100 randomly selected nanoflakes of 100, 250 and 400 W samples respectively.

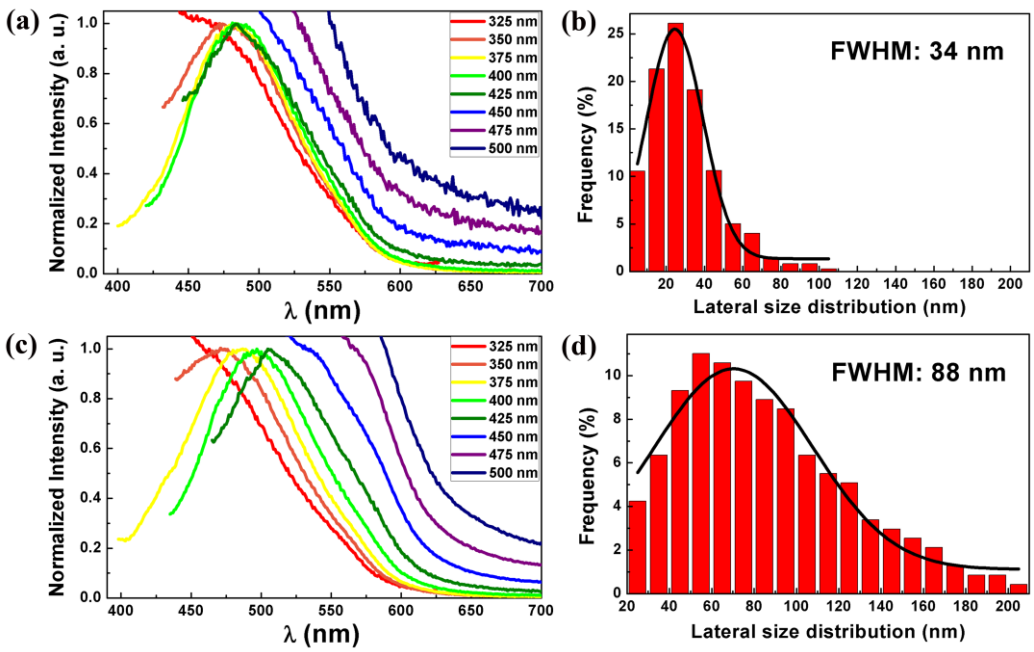

Figure 6. PL properties of MoS_2 nanoflakes. (a) and (c) PL spectra of MoS_2 nanoflakes suspended in NMP solution at different excitation wavelengths (ranging from 325 nm to 500 nm) ((a): 250 W; (c): 400 W). (b) and (d) Lateral size distributions of MoS_2 nanoflakes obtained from TEM images (based on more than 300 randomly selected nanoflakes) ((b): 250 W; (d): 400 W).